Satellite Products and Services Review Board

Algorithm Theoretical Basis Document:

Imaging Wind and Rain Airborne Profiler

(IWRAP) Retrievals

Compiled by:
NOAA/NESDIS/STAR Ocean Surface Winds Team

Version 5.0

April, 2026

AUTHORS:

Paul S. Chang (NOAA/NESDIS/STAR): *paul.s.chang@noaa.gov*
Zorana Jelenak (UCAR): *zorana.jelenak@noaa.gov*
Joseph Sapp (Global Science & Technology): *joe.sapp@noaa.gov*
Casey Shoup (Global Science & Technology): *casey.shoup@noaa.gov*

LIST OF CHANGES

DOCUMENT TITLE: ATBD – IWRAP Retrievals			
DOCUMENT CHANGE HISTORY			
Revision No.	**Date**	**Revision Originator Project Group**	**CCR Approval # and Date**
1.0	04/2026	J. Sapp	N/A
2.0	04/2026	J. Sapp	N/A
3.0	04/2026	J. Sapp	N/A
4.0	04/2026	J. Sapp	N/A
5.0	04/2026	J. Sapp	N/A

LIST OF CHANGES

DOCUMENT TITLE: ATBD – IWRAP Retrievals					
LIST OF CHANGE-AFFECTED PAGES/SECTIONS/APPENDICES					
Version Number	**Date**	**Changed By**	**Page**	**Section**	**Description of Change(s)**
1.0	04/2026	J. Sapp		All	Initial design of the dual-frequency (C/Ku) conical scanning architecture for inner-core hurricane studies.
2.0	04/2026	J. Sapp		3	Development of the high-wind Geophysical Model Function (GMF) for co-polarized backscatter.
3.0	04/2026	J. Sapp		1, 2	Implementation of pulse compression (LFM chirps) to enhance sensitivity and range resolution.
4.0	04/2026	J. Sapp		3	Characterization of non-saturating cross-polarized (VH) ocean surface backscatter in extreme winds.
5.0	04/2026	J. Sapp		All	Integration of frequency agility (ARENA 522), NRT 3D wind retrieval processing, automated drift-dependent pointing calibration.

TABLE OF CONTENTS

LIST OF ACRONYMS

3D-VAR: Three-Dimensional Variational Data Assimilation
ABL: Atmospheric Boundary Layer
ARENA: Adaptive Reconfigurable Embedded Network Appliance
ASCAT: Advanced Scatterometer
ATBD: Algorithm Theoretical Basis Document
CBLAST: Coupled Boundary Layers and Air-Sea Transfer
CTS: Coherent Turbulent Structure
DA: Data Assimilation
EMC: Environmental Modeling Center
FFT: Fast Fourier Transform
GMF: Geophysical Model Function
HBL: Hurricane Boundary Layer
HIWRAP: High-Altitude IWRAP
IMU: Inertial Measurement Unit
IWRAP: Imaging Wind and Rain Airborne Profiler
LFM: Linear Frequency Modulation
MIRSL: Microwave Remote Sensing Laboratory
NDBC: National Data Buoy Center
NESDIS: National Environmental Satellite, Data, and Information Service
NetCDF: Network Common Data Form
NHC: National Hurricane Center
NOAA: National Oceanic and Atmospheric Administration
NRCS: Normalized Radar Cross-Section
NRT: Near-Real-Time
OSVW: Ocean Surface Vector Wind
OSWT: Ocean Surface Winds Team
PSD: Power Spectral Density
RPM: Revolutions Per Minute
SAR: Synthetic Aperture Radar
SatCom: Satellite Communications
SDR: Software-Defined Radar

SFMR: Stepped Frequency Microwave Radiometer

SNR: Signal-to-Noise Ratio

STAR: Center for Satellite Applications and Research

TC: Tropical Cyclone

TKE: Turbulent Kinetic Energy

VAD: Velocity Azimuth Display

Section 1

Instrument Description

1.1. Instrument Overview and Technical Specifications

The Imaging Wind and Rain Airborne Profiler (IWRAP) is a dual-frequency, high-resolution (C- and Ku-band) Doppler radar system designed for the environmental characterization of Tropical Cyclones (TCs). The system conically scans the ocean surface and intervening atmosphere from the NOAA WP-3D "Hurricane Hunter" aircraft to retrieve three-dimensional wind structure and surface backscatter.

The system utilizes a conically scanning pencil-beam antenna rotating at 60 RPM, providing a 360° azimuthal look every second. IWRAP simultaneously profiles at two Earth-incidence angles (typically 30° and 50°) using 30 m range gates. The digital subsystem, centered on the Tomorrow.io Adaptive Reconfigurable Embedded Network Appliance (ARENA 522), enables frequency agility and multi-beam diversity via Linear Frequency Modulated (LFM) chirps and matched filtering to maximize signal-to-noise ratio (SNR). The ARENA 522 software-defined radar (SDR) platform supports arbitrary transmit waveform generation, real-time matched filtering, pulse-pair computation, and spectral processing, all performed on a reconfigurable FPGA architecture (Sapp et al. 2023; Sapp et al. 2025).

Table 1-1: IWRAP Instrument Specifications

Parameter	**C-band**	**Ku-band**
Frequency Range	4.9–5.5 GHz	12.89–13.95 GHz
Polarization	VV, HH, VH, HV	VV, HH, VH, HV
Pulse Type	LFM Chirp / Short Pulse	LFM Chirp / Short Pulse
Range Resolution	30 m	30 m
Incidence Angles	30°, 50°	30°, 50°
Antenna Rotation	60 RPM	60 RPM
3 dB Beamwidth	~5°	~2°

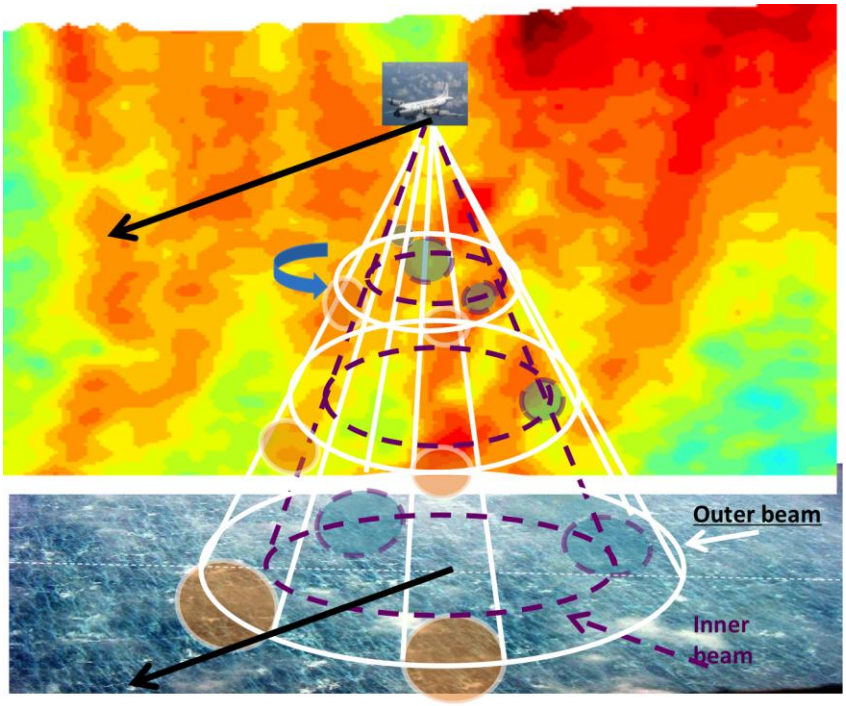

Figure 1.1: IWRAP conical scanning measurement geometry. The system simultaneously profiles at two Earth-incidence angles (inner beam at 30° and outer beam at 50°) from the NOAA WP-3D aircraft. The conically scanning pencil-beam antenna rotates at 60 RPM, providing 360° azimuthal coverage every second.

The IWRAP system is designed to provide horizontal grid increments of at least 125 m and vertical resolutions of at least 30 m. It maintains wind retrieval sensitivity exceeding 70 m/s while resolving the "boundary layer gap" (the lowest 500 m) where surface clutter historically precluded accurate measurements.

1.2. Instrument Heritage and Technological Evolution

The IWRAP system is the culmination of several generations of airborne scatterometry and profiling developed by the Microwave Remote Sensing Laboratory (MIRSL) at the University of Massachusetts Amherst. Its technical lineage begins with the C-band scatterometer (CSCAT), which introduced the frequency-steered microstrip array antenna architecture (McLaughlin et al. 1991). CSCAT proved the feasibility of electronically scanning elevation angles (20° to 50°) while mechanically rotating in azimuth. Refinements led to the dual-frequency CSCAT/KUSCAT precursor systems, which established the baseline for rapid conical scanning and the integration of active radar backscatter with passive radiometer data (Carswell et al. 1999).

The transition to IWRAP introduced Doppler profiling capabilities and higher spatial resolution. Initially, IWRAP utilized a time-multiplexed switching system, which limited multi-beam sampling due to a 1/N duty cycle penalty. The most significant modern evolution occurred in 2020–2022 with the integration of the ARENA 522 digital subsystem. This upgrade enabled frequency agility, permitting simultaneous transmission on multiple beams and the real-time

processing of full Doppler spectra. This technological leap transitioned IWRAP from a post-flight research instrument to a near-real-time (NRT) operational system capable of delivering 3D wind vectors to the National Hurricane Center during flight missions (Sapp et al. 2025).

1.3. Field Campaigns and Operational History

Since its inception, IWRAP has been deployed in numerous research and operational field campaigns targeting tropical and extratropical cyclones:

- **Early TC Research (2002–2004):** Missions through Hurricanes Lili (2002) and Isabel (2003) established baseline boundary layer profiling, rain effect characterization, and limitations on high-wind scatterometry at co-polarization (Fernandez et al. 2004, 2005).
- **CBLAST and Extreme Winds (2005):** Hurricane Rita (2005) provided the first high-resolution observations of coherent turbulent structures (CTSs) and eyewall kinetic energy backscatter during an eyewall replacement cycle (Sroka and Guimond 2021).
- **High-Wind GMF Development (2005–2017):** Dedicated missions targeted high-wind regimes in extratropical and tropical cyclones to characterize the radar backscatter response and improve Geophysical Model Functions (GMFs). This period saw significant advancements in dual-polarization observations (Dvorsky 2012), low incidence angle NRCS characterization (Sapp et al. 2013, 2015), and the study of non-saturating cross-polarized signals (Sapp 2015; Sapp et al. 2016), frequently validated against spaceborne SAR (Sapp et al. 2020).
- **Next-Generation Scatterometer Research (2015–2018):** Flights through tropical and extratropical cyclones, including Hurricanes Patricia (2015) and Matthew (2016), focused on cross-polarized (VH) NRCS measurements for next-generation scatterometer risk-reduction (Sapp et al. 2016, 2018).
- **NRT Operational Era (2020–Present):** Recent deployments in Hurricanes Dorian (2019), Ida (2021), Ian (2022), and Lee (2023) demonstrated the frequency-agile NRT processing stream, providing high-resolution 3D winds within the eye-eyewall interface for operational forecasting at NHC.

Figure 1.3 illustrates the NRT IWRAP product development roadmap across four seasons of progressive capability maturation. The 2021 early-development stage established NRT 3D winds from Ku-band. The 2022 intermediate stage added OSVW retrievals. The 2023 late-development stage integrated C-band 3D winds, OSVW combined with rain rate, and multi-channel blending. The 2024 early-application stage focused on error characterization, blended 3D wind and OSVW products, and comprehensive validation.

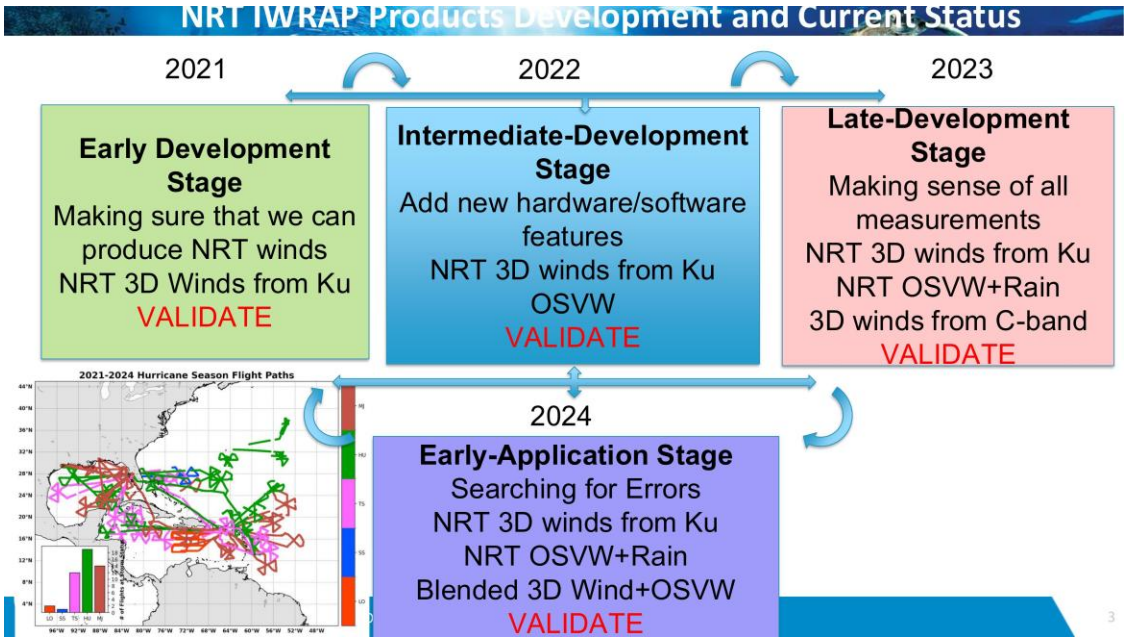

Figure 1.3: NRT IWRAP product development and current status timeline, showing progressive capability maturation from 2021 (early development) through 2024 (early application), with validation campaigns in Hurricanes Ida, Ian, Lee, Helene, and Milton.

1.4. Instrument Ground Calibration

Before and after each deployment, ground calibration is performed on the radar systems. Each antenna is removed and various parameters are measured at each transmit frequency with calibrated test equipment. In particular: transmit power at the output port to the antenna, relative to that which is measured by the system through the internal calibration loop; receiver gain from the antenna input at the front-end to the digital receiver; system noise power when the output port to the antenna is terminated with a matched load; and the antenna "zero" position.

Any differences in system noise power between digital receiver channels greater than 1 dB are adjusted in hardware before calibration is complete, minimizing signal corruption due to leakage from one signal to another across the digital receiver channels.

Every time the antenna or mounting structure is removed and re-installed, the antenna "zero" position along the fuselage must be re-derived. The most reliable method is through a pointing angle calibration with real data. Sapp et al. (2024) demonstrated that because the antenna mounting flexes slightly during flight, the pointing angles contain an attitude-dependent drift. Their methodology derives the pointing angle correction by establishing a geometric relationship between the measured NRCS pattern as a function of look angle and matching it to the ocean surface backscatter model, accounting for roll- and pitch-dependent offsets. Similarly, the NRCS must have a final calibration applied to account for system losses (Sapp et al. 2013; Sapp 2015).

Section 2

3D Wind Retrieval Algorithm Description

2.1. Processing Outline

Extraction of 3D wind vectors from IWRAP follows a sequential processing pipeline:

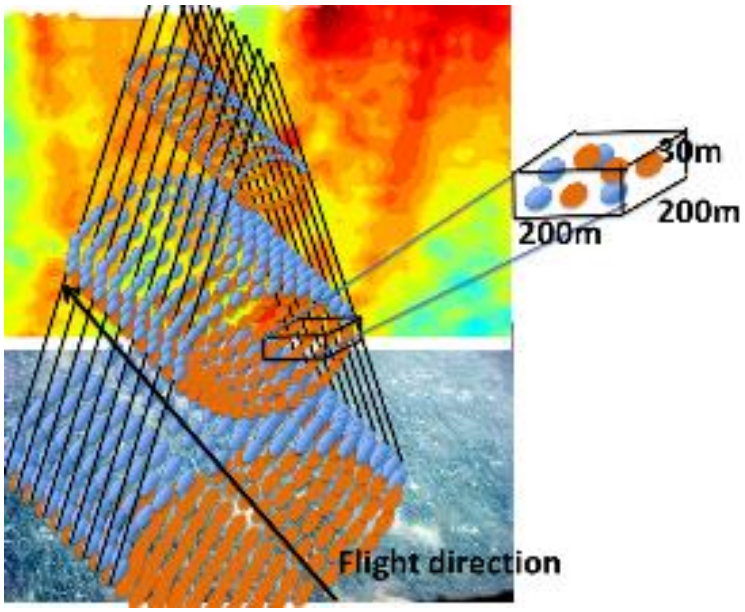

Figure 2.1: IWRAP NRT observation geometry. 3D wind and reflectivity profiles are retrieved along the nadir track at 30 m vertical and 150 m along-track resolution. The ku1 channel (LFM chirp) provides profiles from 1.5 km below the aircraft to 30 m above the surface, while the ku2 channel (short pulse) profiles from 120 m below the aircraft to 30 m above the surface. Maximum swath width is approximately 2–3 km.

1. **Matched Filtering and Geolocation:** Raw digital samples are range-compressed using matched filtering of the LFM chirp waveform. Geolocation of each range gate utilizes aircraft IMU/GPS data to transform radar coordinates into an Earth-referenced frame.
2. **Doppler Velocity Estimation:** Radial velocities are derived from covariance estimators (pulse-pair) or spectral FFT analysis. The contemporary spectral approach performs a 128-point FFT to generate the power spectral density (PSD) at each range gate, enabling objective surface clutter rejection.
3. **Quality Control:** Non-meteorological signals (surface clutter, noise, sidelobe leakage) are identified and excised through objective thresholds and image processing techniques. A Gaussian fitting algorithm isolates the atmospheric Doppler shift from the composite spectrum.
4. **Vector Synthesis:** Independent radial Doppler measurements are synthesized into a coherent 3D Cartesian wind field (u, v, w) using either variational (3D-VAR) or along-track cell methods.

2.2. Legacy Covariance-Based Retrieval (Pulse-Pair)

Historically, wind vector retrieval relied upon covariance-based data processing known as the pulse-pair technique. This estimator calculates the first moment of the Doppler spectrum from the phase of the complex autocorrelation of successive returns. While computationally efficient, this methodology is subject to severe biases in the lower boundary layer. The antenna main beam and sidelobes inevitably intersect the ocean surface, which often possesses Doppler velocities significantly different from precipitation volume backscatter. The resulting composite Doppler spectrum is skewed toward the stationary (zero-Doppler) surface signals, inducing a negative bias in wind speed estimates and precluding accurate retrievals at altitudes below approximately 500 m. Echoes from a sidelobe directed at nadir also inhibit retrievals at an altitude corresponding to the aircraft altitude, projected onto the beam.

Early 3D wind retrievals were limited to 500 m above the surface for these reasons. This boundary layer gap was a critical limitation because the lowest 500 m of the hurricane boundary layer is where the strongest wind gradients and the most operationally significant winds occur.

2.3. Contemporary Spectral-Based Retrieval

To resolve the boundary layer data gap, contemporary methodologies utilize full spectral analysis to generate the power spectral density (PSD) at each range gate. A 128-point FFT is applied to the complex voltage time series from each range gate, producing a Doppler spectrum that separately resolves the atmospheric signal from the ocean surface clutter (Sapp et al. 2025).

A Gaussian fitting algorithm identifies and masks frequency bins corresponding to the relatively stationary ocean surface, isolating the true atmospheric Doppler shift. The first moment of the clutter-removed spectrum yields the radial velocity estimate for that range gate. This methodology permits high-resolution wind profiling down to 30 m above the surface, facilitating examination of coherent turbulent structures (CTSs), turbulent rolls, and fine-scale eyewall dynamics that were previously unresolvable. The measurement sensitivity covers rain rates between approximately 7 mm/hr and 90 mm/hr.

IWRAP operates with two Ku-band channels that provide complementary coverage. The ku1 channel transmits a 10 μs LFM chirp at approximately 50° incidence, providing enhanced sensitivity and profiles from 1.5 km below the aircraft down to 30 m above the surface; however, the transmit pulse length introduces a blind range of approximately 1.5 km. The ku2 channel transmits a short (250 ns) pulse at approximately 30° incidence with a blind range of only 120 m below the aircraft, enabling profiling of the near-aircraft region. Together, the two channels provide continuous vertical coverage from just below the aircraft to 30 m above the ocean surface. During the 2021 Hurricane Ida flights, the spectral processor was successfully demonstrated on three eyewall passes on August 29th, confirming its capability to resolve the lowest levels of the hurricane boundary layer in a Category 4 storm (Sapp et al. 2025). More recently, complementary transmit waveforms have been added to sample near the aircraft on the outer beam (ku3) and near

the surface on the inner beam (ku4). ku3 is a 250 ns pulse transmitted at approximately 50° incidence, and ku4 is a 10 µs chirp transmitted on the 30° beam.

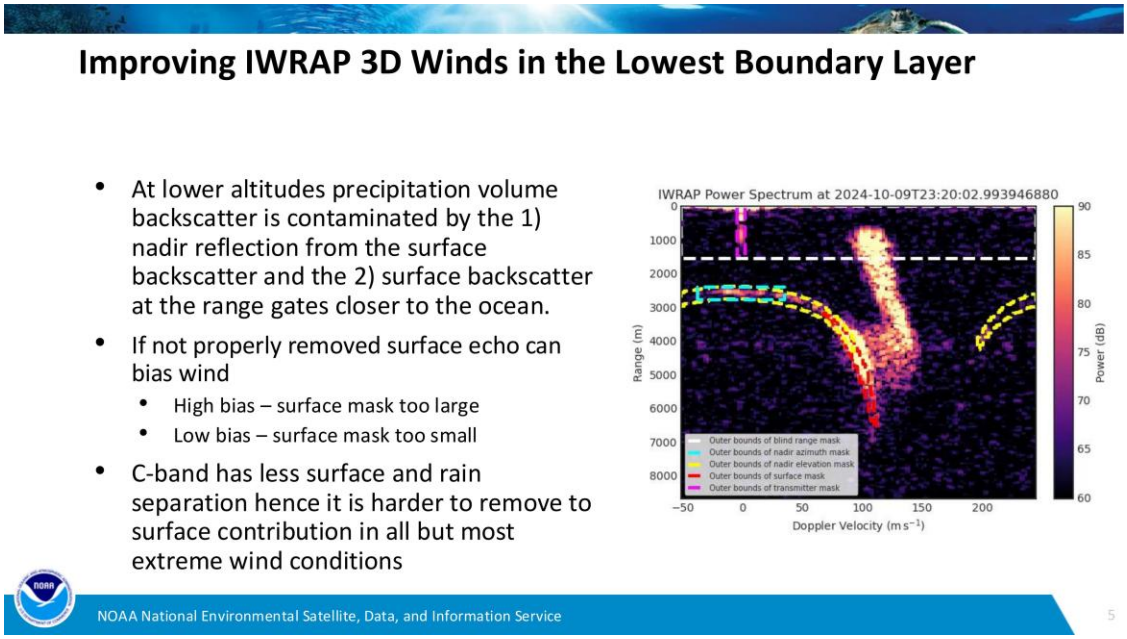

Figure 2.3a: Spectral clutter rejection methodology. Right: IWRAP Ku-band power spectrum (range vs. Doppler velocity) showing the atmospheric precipitation signal, nadir echo, and ocean surface backscatter. The dashed boundaries delineate the surface clutter masks applied to isolate the meteorological Doppler signal. If the surface echo is not properly removed, it biases the retrieved wind: a mask that is too large removes valid atmospheric signal (low bias), while a mask that is too small allows surface contamination (high bias).

The most unique aspect of the IWRAP radar is its advanced radar control and data acquisition system, which collects both in-phase (I) and quadrature (Q) signals for the entire observational profile. This allows the full Doppler power spectrum to be derived by applying a series of FFTs on every single range gate. Figure 2.3b illustrates this principle by showing individual Doppler spectra at four representative altitudes during Hurricane Ida (2021). At 910 m altitude, only the rain signal is present as a single well-defined peak. At 340 m, the rain peak remains dominant. At 80 m, a second peak corresponding to the ocean surface begins to appear alongside the rain signal. At 0 m (the ocean surface), the surface signal dominates. This altitude-dependent evolution of the spectrum is the physical basis for the spectral clutter rejection technique.

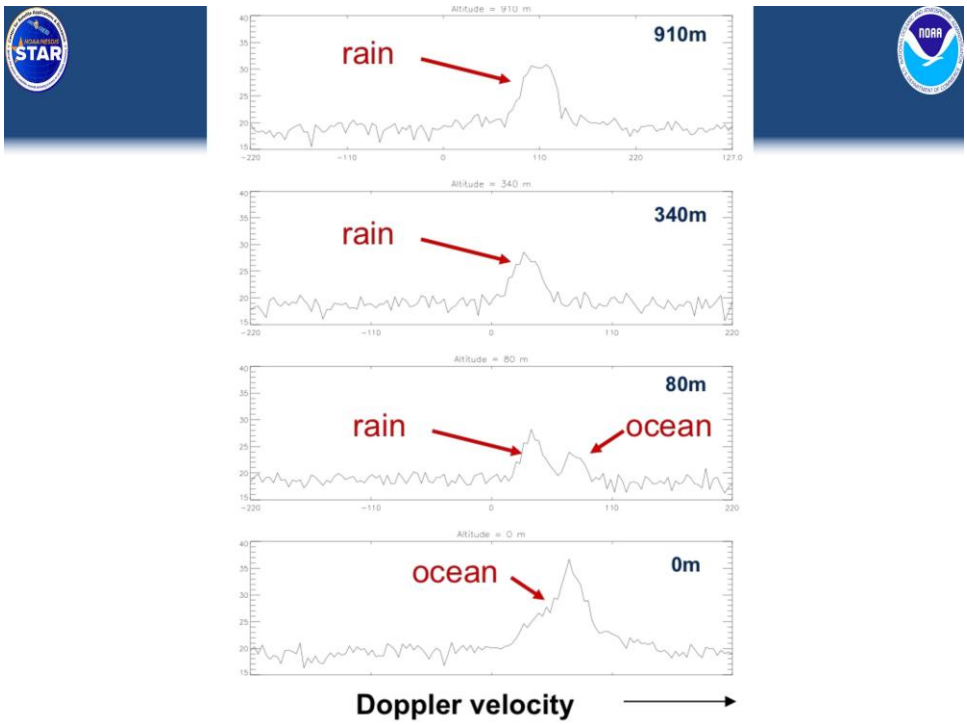

Figure 2.3b: IWRAP Doppler spectra at four altitudes during Hurricane Ida (August 29, 2021). At 910 m and 340 m, only the rain precipitation signal is present. At 80 m, the ocean surface signal begins to emerge as a distinct second peak. At 0 m, the surface echo dominates. This altitude-dependent spectral evolution demonstrates how the rain and surface signals can be separated in Doppler space, enabling wind retrieval down to 30 m above the ocean.

Figure 2.3c shows the full spectral processing implementation. For each range gate, the power spectrum is computed and a Gaussian fitting algorithm is applied to identify and separate the rain and surface components. At ranges well above the surface (e.g., 300 m, 450 m), only the precipitation peak requires fitting. Near the surface (e.g., 1890 m range, 2400 m range), the algorithm must delineate between the precipitation and ocean surface peaks, applying the clutter mask to isolate the atmospheric Doppler velocity. The fitted Gaussian parameters (peak power, center velocity, spectral width) provide quality metrics for each retrieval.

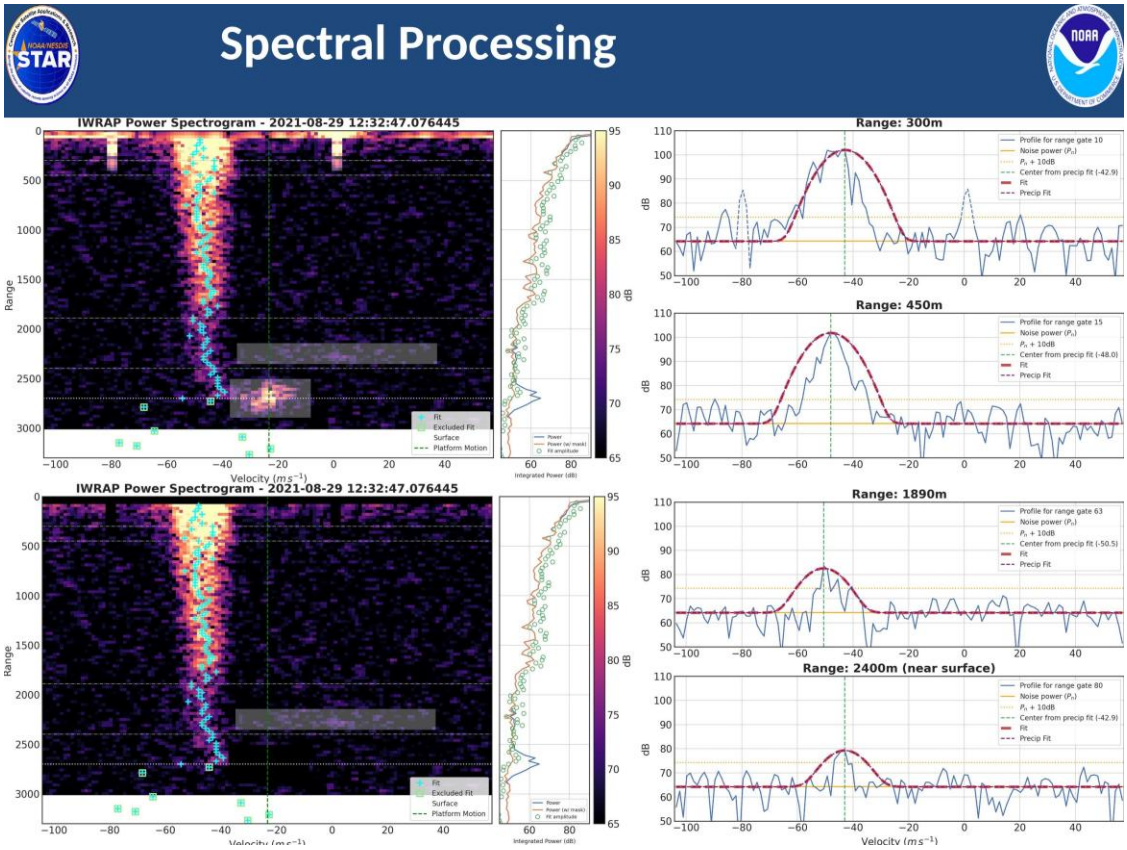

Figure 2.3c: Spectral processing of IWRAP data during Hurricane Ida (August 29, 2021, 12:32:47 UTC). Left panels: full power spectrograms (range vs. Doppler velocity) for Ku1 (top) and Ku2 (bottom) channels, with surface clutter mask boundaries overlaid. Right panels: individual Doppler spectra (blue) with Gaussian fits (red dashed) at four representative ranges (300 m, 450 m, 1890 m, and near-surface at 2400 m), showing the progressive emergence of the ocean surface peak at lower altitudes.

The spectral approach is particularly advantageous at the two IWRAP incidence angles (30° and 50°). At 50° incidence, the ocean surface return is separated in Doppler space from the atmospheric signal by a greater margin, enabling cleaner clutter rejection. At 30° incidence, the surface and atmospheric signals overlap more, but the higher-SNR conditions at this angle provide complementary constraints on the horizontal wind components. C-band presents an additional challenge: the separation between the surface echo and precipitation signal is smaller than at Ku-band, making it harder to remove the surface contribution in all but the most extreme wind conditions.

2.3.1 Doppler Velocity De-Aliasing

A significant technical challenge emerged during high-intensity storm flights, particularly those into Hurricane Milton (2024), where Doppler aliasing contaminated the IWRAP velocity data. In these conditions, the instrument's configured Pulse Repetition Frequency (PRF) was insufficient to unambiguously measure the extreme wind speeds present. The maximum unambiguous velocity is determined by the PRF and radar wavelength; for the frequency and PRF settings used during

Milton, this limit was approximately 58.1 m/s. Wind speeds observed in the eyewall exceeded this threshold, causing the measured Doppler velocities to "wrap around" and appear as incorrect, lower-velocity values moving in the opposite direction.

This aliasing resulted in erroneously flagged or entirely discarded data within the most critical regions of the storm, such as the eyewall, compromising the integrity of the wind field analysis. Figure 2.3d illustrates this problem: the along-track horizontal wind curtain from Hurricane Milton shows extensive data gaps and artifacts in the eyewall region where the highest winds occur.

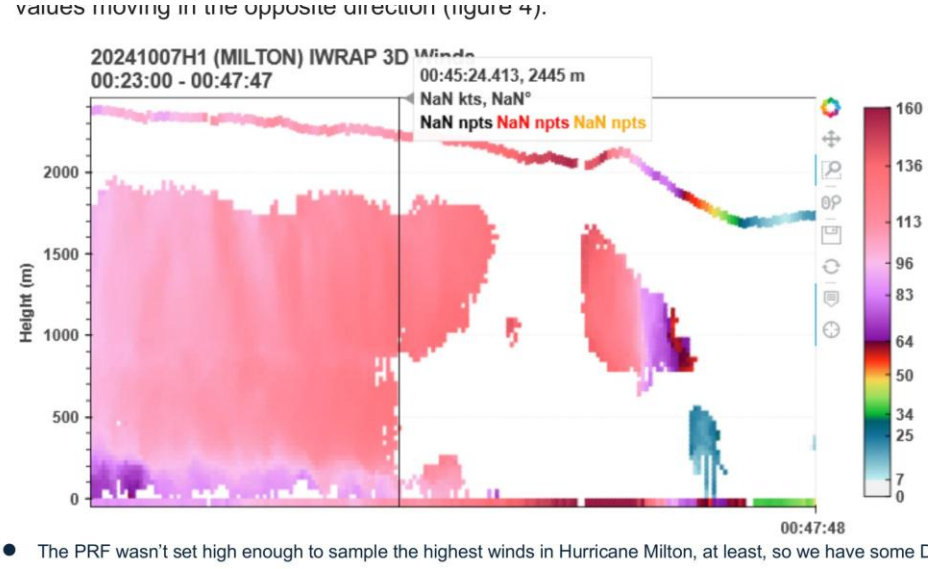

Figure 2.3d: IWRAP 3D wind speed curtain from Hurricane Milton (October 7, 2024). The PRF was not set high enough to sample the highest winds, resulting in Doppler aliasing. The unambiguous velocity is approximately 58.1 m/s for this frequency and PRF configuration. Aliasing causes excessively flagged retrievals inside the eyewall where the most operationally significant winds occur.

To address this issue, a modified version of the established UNRAVEL (Louf et al., 2020) algorithm was implemented to de-alias the IWRAP Doppler velocity data. The solution was designed with specific trade-offs: the de-aliasing code is only executed when flight-level winds exceed half of the unambiguous velocity, which avoids introducing unnecessary processing artifacts when aliasing is not present. However, this conditional approach introduces a dependency on the availability and accuracy of flight-level wind speed data to trigger the correction. Figure 2.3e shows the results of the de-aliasing applied to the same Hurricane Milton data, demonstrating recovery of the aliased velocity field.

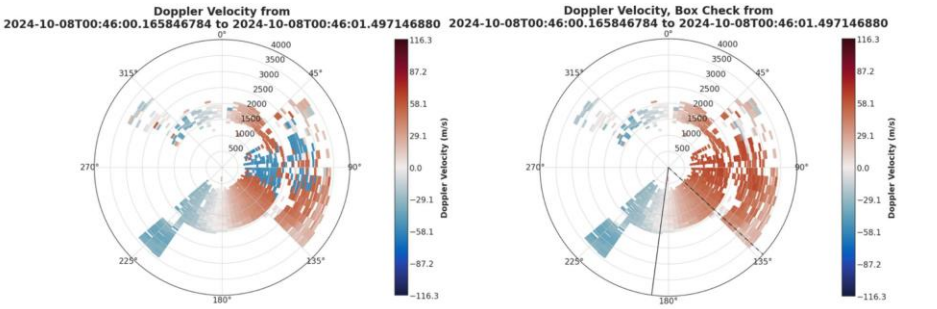

- Utilize modified UNRAVEL algorithm
- Only run the dealiasing code if the flight-level winds are greater than ½ the unambiguous velocity
- Pro: Avoids some unnecessary risk
- Con: Introduces dependence on flight-level wind speed

Figure 5

Figure 2.3e: Doppler velocity de-aliasing results for Hurricane Milton (October 8, 2024). Left: original Doppler velocity field showing aliased (wrapped) velocities at high wind speeds. Right: de-aliased velocity field after application of the modified UNRAVEL algorithm, recovering the true velocity structure. The de-aliasing is conditionally applied only when flight-level winds exceed half the unambiguous velocity (~29 m/s).

2.4. Vector Synthesis Methodologies

2.4.1 Velocity-Azimuth Display (VAD) Principles

Both vector synthesis methods are grounded in the Velocity-Azimuth Display (VAD) technique. The measured radial velocity v_r at each range gate is a function of the local 3D wind vector (u, v, w) projected onto the radar line-of-sight direction, plus the hydrometeor terminal fall speed v_t:

$$v_r = u \sin\theta \cos\phi + v \sin\theta \sin\phi + (w - v_t)\cos\theta$$

where θ is the incidence angle and ϕ is the azimuth angle. As the antenna rotates through 360°, the radial velocity traces a sinusoidal pattern whose amplitude and phase encode the horizontal wind speed and direction, respectively. The vertical velocity and terminal fall speed contribute a constant offset. By fitting this sinusoidal model to the observed radial velocities at each altitude, the 3D wind vector is retrieved.

2.4.2 Variational 3D-VAR Methodology

The variational methodology synthesizes the 3D wind field (u, v, w) by minimizing a global cost function J:

$$J = J_o + J_m + J_s$$

- **Observation Term (J_o):** Minimizes the discrepancy between measured radial velocities ($v_{r,obs}$) and the projected wind vectors, incorporating hydrometeor terminal fall speed derived from reflectivity.
- **Mass Continuity Constraint (J_m):** Enforces anelastic mass continuity, allowing the derivation of vertical velocity (w) from the horizontal wind field divergence.
- **Smoothness Constraint (J_s):** Utilizes Tikhonov regularization to suppress noise while preserving coherent structural integrity. This constraint prevents spatially unphysical oscillations in the retrieved wind field.

The 3D-VAR methodology produces the highest-fidelity wind fields and is well suited for research applications where post-flight processing time is acceptable. This approach synthesizes all available Doppler measurements across the full conical scan into a single 3D Cartesian grid, capturing the complete spatial structure of the hurricane boundary layer (Guimond et al. 2014).

2.4.3 Along-Track Cell Vector Synthesis (NRT)

An alternative methodology is employed for near-real-time (NRT) dissemination. This approach prioritizes computational throughput by grouping Doppler observations into independent grid cells along the flight track. Synthesis is performed for each cell independently using a weighted least-squares minimization of radial velocity observations. This method omits cross-track binning, providing robust horizontal wind components u and v for immediate operational dissemination to the National Hurricane Center (NHC).

The NRT algorithm was implemented as part of the ARENA 522 upgrade and transmits wind products via the WP-3D satellite communications (SatCom) link during flight. Typical latency from observation to NHC delivery is defined relative to the conclusion of a singular pass through the storm. The cell-based approach sacrifices some spatial resolution relative to the 3D-VAR product but provides operationally relevant wind information within the timeframe required for tropical cyclone forecasting decisions (Sapp et al. 2025).

2.5. Multi-Channel Blending

A next-generation profiler should operate at two or more different frequencies, ideally with at least one non-attenuating channel. IWRAP satisfies this requirement through its dual-frequency (C- and Ku-band), dual-incidence-angle (30° and 50°) architecture. Each channel combination offers distinct advantages and limitations in terms of sensitivity, attenuation, and surface clutter separation. Blending these channels produces a composite wind field that exceeds the capability of any single channel.

Figure 2.5 illustrates the complementary nature of the three primary retrieval channels: Ku-band at 30°, Ku-band at 50°, and C-band at 50° incidence. Ku-band at 30° provides the highest sensitivity in moderate precipitation but suffers from attenuation in heavy rain cores. Ku-band at

50° offers better surface clutter separation due to the wider Doppler offset between the atmospheric and surface signals. C-band provides the least attenuation in precipitation, although its smaller Doppler separation between surface and rain echoes makes clutter removal more challenging. The choice of incidence angle is critical for surface contamination removal, and narrow beams are essential for minimizing sidelobe-induced clutter.

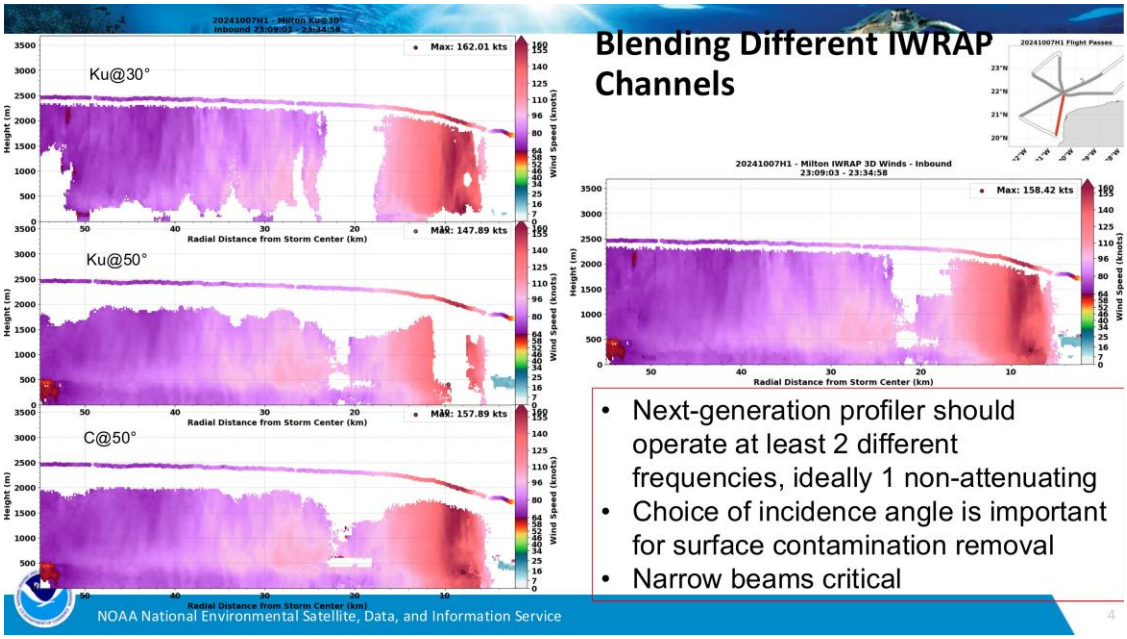

Figure 2.5: Blending different IWRAP channels. Left panels show along-track curtains of horizontal wind speed from Ku-band at 30°, Ku-band at 50°, and C-band at 60° during Hurricane Milton (2024). Right panel shows the blended multi-channel 3D wind composite. Each channel contributes unique coverage depending on rain rate, incidence angle, and frequency-dependent attenuation characteristics.

2.6. Validation

Validation of IWRAP wind retrievals utilizes a triple collocation framework incorporating GPS dropsondes, spaceborne SAR imagery, and numerical model output. Spectral retrievals demonstrate superior agreement with dropsondes at altitudes below 500 m compared to legacy pulse-pair estimates, confirming the effectiveness of the clutter rejection methodology.

Comparisons during Hurricane Dorian (2019) indicated an RMSE of approximately 2.3 m/s for horizontal wind components. Additional validation during Hurricanes Ida (2021) and Ian (2022) demonstrated consistent performance across storm intensities ranging from Category 1 to Category 4 conditions. The NRT wind products showed agreement with 3D-VAR products at the grid scales relevant to operational forecasting, with differences primarily attributable to the reduced spatial averaging in the cell-based approach.

Figure 2.6a presents a scatter comparison of IWRAP 30° channel retrievals at the highest altitude bin against collocated flight-level horizontal winds from the NOAA WP-3D aircraft. The

comparison encompasses 17,570 matchup points across multiple hurricane penetrations. The mean bias is 0.23 m/s with a standard deviation of 2.32 m/s, demonstrating excellent agreement between the IWRAP Doppler-derived winds and the in-situ aircraft measurements across the full intensity range observed.

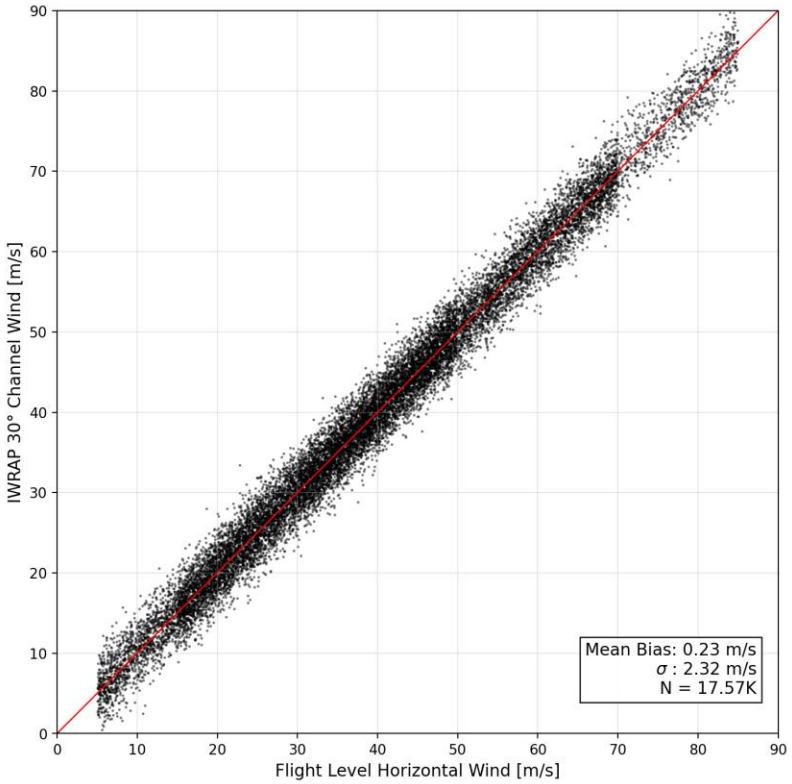

Figure 2.6a: Scatter comparison of IWRAP 30° channel wind retrievals (highest altitude bin) versus flight-level horizontal winds from the NOAA WP-3D aircraft. Mean bias is 0.23 m/s, standard deviation is 2.32 m/s, N = 17,570. The red line indicates the 1:1 reference.

Figure 2.6b presents a detailed comparison of IWRAP 3D wind profiles with collocated GPS dropsonde measurements within a single pass through Hurricane Milton (2024). The upper panels display the along-track curtain of horizontal wind speed for inbound (approximately 300 profiles) and outbound (approximately 270 profiles) legs. The lower panels show 2D histograms of horizontal wind speed as a function of altitude, with dropsonde profiles overlaid. This comparison provides an opportunity to re-examine the classical dropsonde-based boundary layer wind profile characterizations (e.g., Franklin et al. 2003) with the unprecedented vertical resolution afforded by IWRAP.

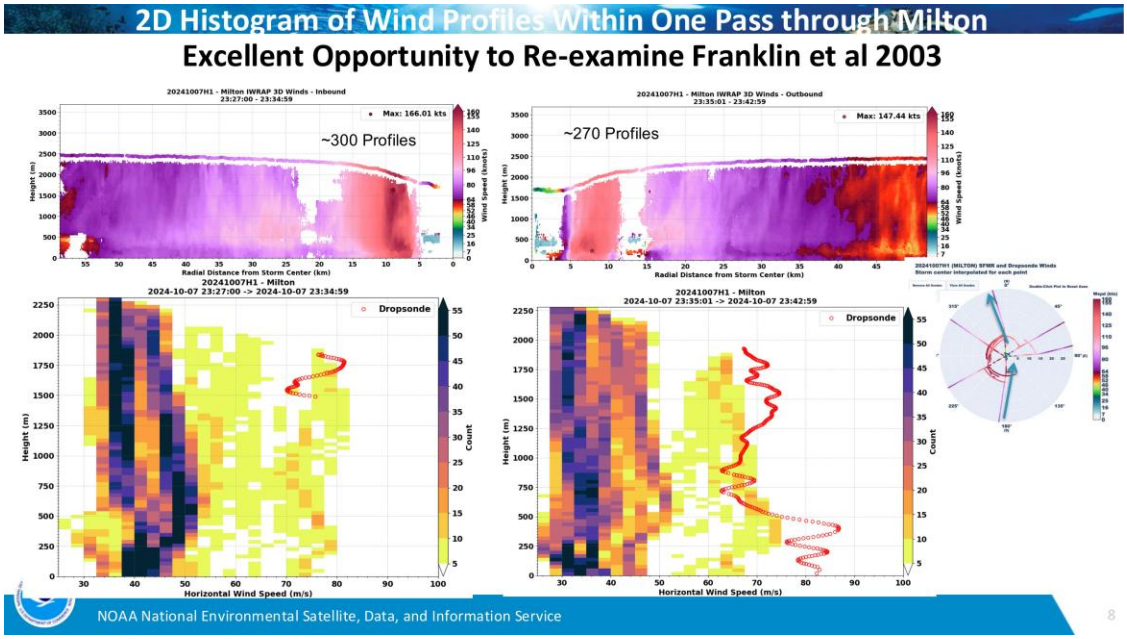

Figure 2.6b: 2D histogram of IWRAP wind profiles within a single pass through Hurricane Milton (2024), with collocated GPS dropsonde profiles (red curves) overlaid. Upper panels: along-track curtains of horizontal wind speed for inbound (~300 profiles, max 166 kt) and outbound (~270 profiles, max 147 kt) legs. Lower panels: wind speed as a function of altitude, illustrating the boundary layer structure resolved by IWRAP at 30 m vertical resolution.

2.6.1 Validation Against Tail Doppler Radar (TDR)

A comprehensive comparison with the NOAA WP-3D Tail Doppler Radar (TDR) was performed for the full 2024 hurricane season. TDR produces along-track vertical profiles with 1.5 km spacing and 150 m vertical grid spacing, effectively representing an average wind over a 10 km wide swath across the flight track. For comparison, TDR data are interpolated onto the IWRAP grid. This analysis comprises over 2.5 million matchup points across all 2024 missions.

Figure 2.6c presents histograms of the IWRAP–TDR wind speed and wind direction differences, stratified by aircraft drift direction (positive and negative). This methodology of analysis is particularly useful for determining if there exist pointing angle errors (Sapp et al., 2024; Sapp et al., 2025). The wind speed difference distributions are approximately Gaussian with medians near zero (0.07 m/s for positive drift, –0.47 m/s for negative drift), and the wind direction difference distributions show medians of –2.26° and 3.65°, respectively. The main finding is a correlation between the error characteristics and aircraft drift, which reflects the sensitivity of the wind retrieval to the sampling geometries of the two instruments.

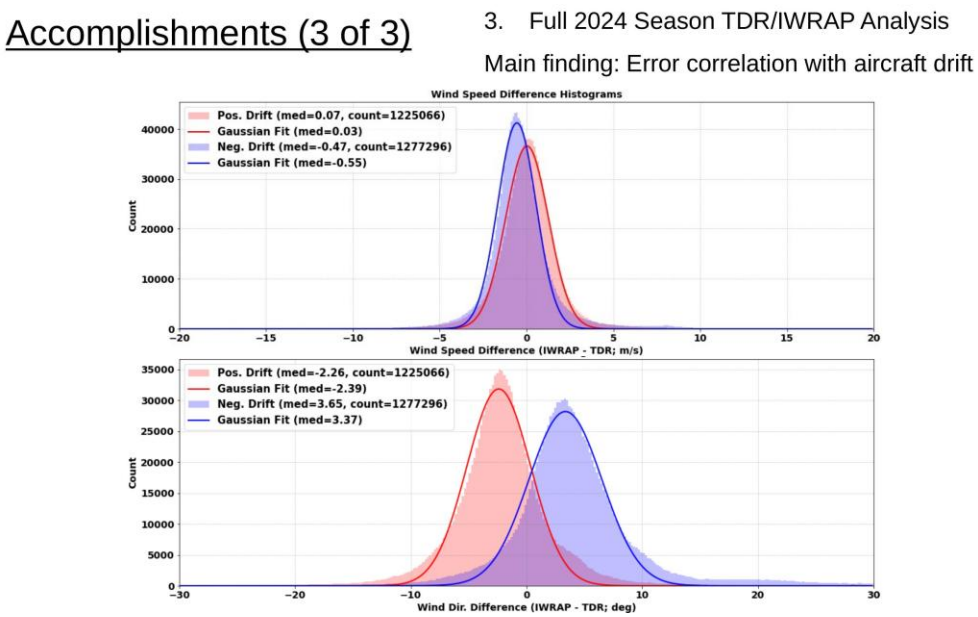

Figure 2.6c: Full 2024 hurricane season IWRAP vs. TDR wind speed difference (top) and wind direction difference (bottom) histograms, stratified by positive drift (red) and negative drift (blue). Gaussian fits are overlaid. Wind speed median differences are 0.07 m/s (positive drift, N = 1,225,066) and –0.47 m/s (negative drift, N = 1,277,296). Wind direction medians are –2.26° and 3.65°, respectively.

Figure 2.6d shows scatter comparisons of IWRAP versus TDR for horizontal wind speed and direction. The wind speed comparison reveals a mean bias of 0.26 m/s with a standard deviation of 3.54 m/s across 266,530 matchup points, with a small linear wind-speed-dependent bias expected due to the differences in measurement resolution between the two instruments. The wind direction comparison shows a mean bias of –0.21° with a standard deviation of 7.00°. Additionally, a comparison using only TDR data below 250 m reveals that TDR does not have sufficient data at these low altitudes for reliable surface wind extrapolation using a logarithmic profile, underscoring the unique value of IWRAP's ability to profile down to 30 m above the ocean surface.

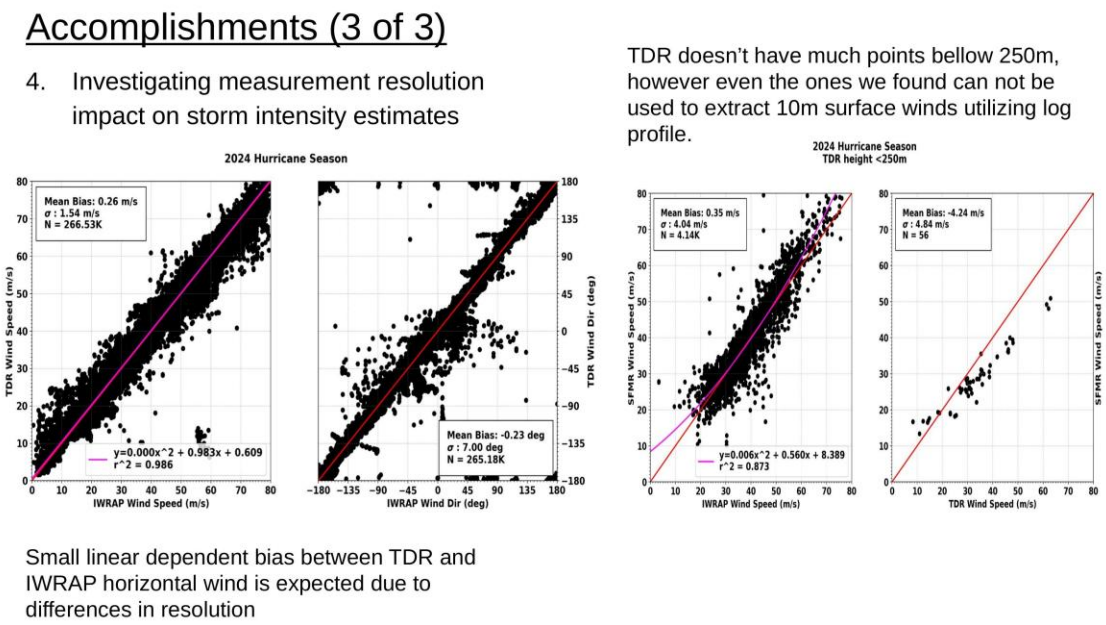

Figure 2.6d: IWRAP vs. TDR scatter comparisons for the full 2024 hurricane season. Left pair: wind speed (mean bias 0.26 m/s, σ = 3.54 m/s, N = 266K) and wind direction (mean bias –0.21°, σ = 7.00°, N = 265K). Right pair: same comparison restricted to TDR heights below 250 m (mean bias 0.35 m/s, σ = 4.04 m/s) and TDR-derived surface wind estimates vs. IWRAP lowest-level winds, demonstrating TDR's limited utility below 250 m.

2.7. Data Products and Data Assimilation Support

The IWRAP processing system generates multiple data products in support of both NRT operational forecasting and research data assimilation (DA) experiments. The primary data products are:

- **3D Horizontal Wind Speed and Direction:** Retrieved at 150 m along-track and 30 m vertical resolution from Ku-band and C-band at both 30° and 50° incidence angles.
- **Vertical Wind:** Derived from the 3D-VAR synthesis through mass continuity constraints, provided at the same 150 m along-track and 30 m vertical resolution.
- **Scatterometry OSVW:** Ocean surface vector winds retrieved from GMF inversion of C-band and Ku-band NRCS at both incidence angles, applicable in no-rain and low-rain regimes.
- **Rain Rate Retrievals:** Derived from C-band and Ku-band reflectivity profiles using established Z–R relationships.

In support of data assimilation experiments, low-resolution IWRAP 3D products have been developed at three spatial resolutions: 1500 m × 150 m, 1500 m × 100 m, and 1500 m × 50 m. For each resolution, the product suite includes tangential wind, radial wind, and wind uncertainties. These products contain blended winds from the two Ku-band channels and are designed to be ingested directly by numerical weather prediction models.

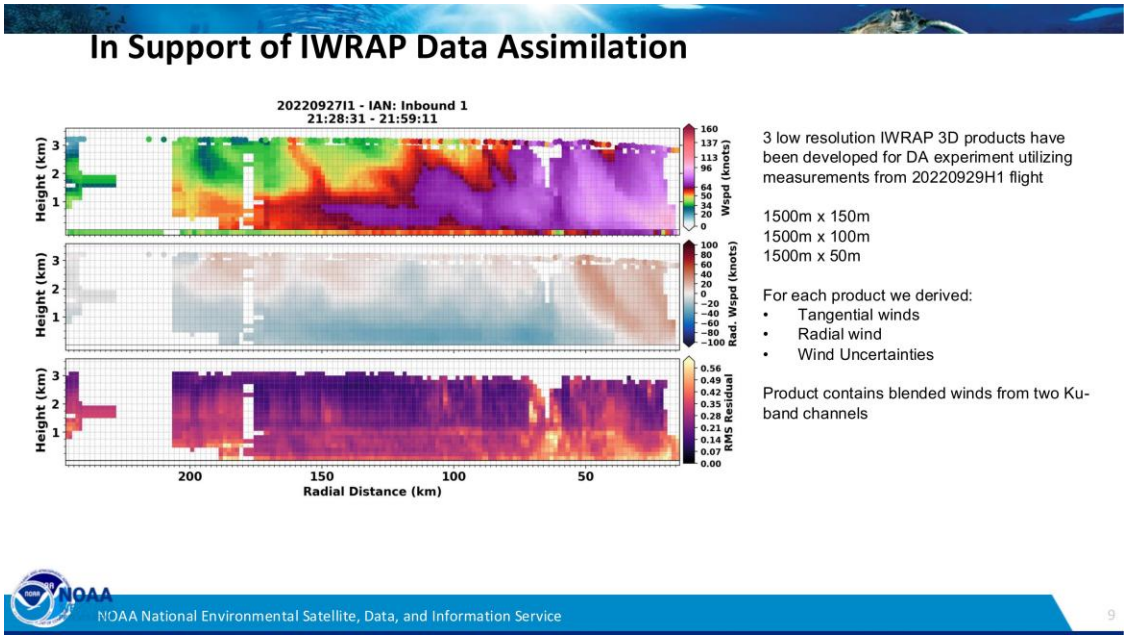

Figure 2.6e: IWRAP 3D products developed for data assimilation, shown for Hurricane Ian (2022). Three panels display tangential wind (top), radial wind (middle), and wind uncertainty (bottom) as a function of radial distance from storm center and altitude. These low-resolution products (1500 m × 150 m) blend measurements from the two Ku-band channels for ingestion into numerical weather prediction models.

2.8. Assumptions and Limitations

The algorithm assumes temporal consistency within each wind vector cell between the times the cell is observed from the forward- and aft-looking beam positions. In practice, this assumption is valid for the time scales of the IWRAP conical scan (approximately 1 s per revolution) relative to the evolving hurricane wind field.

Extreme precipitation often results in significant attenuation of the Ku-band signal, limiting retrievals near the ocean surface in the heaviest rain bands. C-band attenuation is generally minimal except in the most extreme precipitation cores. The dual-frequency design mitigates this limitation by allowing C-band retrievals to fill gaps where Ku-band is attenuated. Incidence angle and sensitivity considerations continue to constrain observations at lower horizontal wind speeds, particularly below 15 m/s.

2.9. Data Access

IWRAP data products are archived in NetCDF-4 format and contain time-referenced, geolocated profiles of Doppler velocity, reflectivity, NRCS, and retrieved 3D wind fields. Preliminary NRT products are transmitted via the WP-3D SatCom network during flights. Full-resolution post-processed products are made available through the NOAA/NESDIS/STAR OSWT data archive at https://manati.star.nesdis.noaa.gov/.

2.10. References

Chu, T., S. J. Frasier, D. E. Fernandez, P. S. Chang, and Z. Jelenak. 2008. "The Impact of Surface Scattering on Ocean ABL Wind Profile Estimates from an Airborne Doppler Radar." Proc. IEEE IGARSS. https://doi.org/10.1109/IGARSS.2008.4779656

Fernandez, D. E., Z. Jelenak, J. R. Carswell, P. S. Chang, and P. G. Black. 2004. "Wind Fields from Hurricane Isabel." Proc. IEEE IGARSS. https://doi.org/10.1109/IGARSS.2004.1370372

Fernandez, D. E., E. M. Kerr, A. Castells, J. R. Carswell, S. J. Shaffer, P. S. Chang, P. G. Black, and F. D. Marks. 2005. "IWRAP: The Imaging Wind and Rain Airborne Profiler for Remote Sensing of the Ocean and the Atmospheric Boundary Layer Within Tropical Cyclones." IEEE Trans. Geosci. Remote Sens., 43(8): 1775–1787. https://doi.org/10.1109/TGRS.2005.851640

Frasier, S. J. and T. Chu. 2009. "Real-Time Airborne Radar Wind-Profiling Algorithm." 34th Conf. on Radar Meteorology, AMS.

Guimond, S. R., L. Tian, G. M. Heymsfield, and S. J. Frasier. 2014. "Wind Retrieval Algorithms for the IWRAP and HIWRAP Airborne Doppler Radars with Applications to Hurricanes." J. Atmos. Oceanic Technol., 31(6): 1189–1215. https://doi.org/10.1175/JTECH-D-13-00140.1

Louf, V., Protat, A., Jackson, R. C., Collis, S. M., & Helmus, J. 2020. “UNRAVEL: A Robust Modular Velocity Dealiasing Technique for Doppler Radar.” J. Atmos. Oceanic Technol., 37(5), 741–758. https://doi.org/10.1175/JTECH-D-19-0020.1

McManus, J. J. 2009. "Implementing Pulse Compression in the IWRAP Airborne Doppler Radar/Scatterometer." MS Thesis, University of Massachusetts Amherst. http://scholarworks.umass.edu/theses/237

Sapp, J. W., Jelenak, Z., & Chang, P. S. 2024. “A Methodology for Calibrating the Pointing Angles of an Airborne Doppler Radar.” IGARSS 2024 - 2024 IEEE International Geoscience and Remote Sensing Symposium, 6546–6549. https://doi.org/10.1109/IGARSS53475.2024.10641007

Sapp, J. W., Jelenak, Z., Chang, P. S., Guimond, S. R., & Carswell, J. R. 2025. “Near-Real-Time IWRAP 3D Wind Retrievals.” Trans. Rad. Sys., 3, 832–842. https://doi.org/10.1109/TRS.2025.3563787

Sroka, S. and S. R. Guimond. 2021. "Organized Kinetic Energy Back-Scatter in the Hurricane Boundary Layer from Radar Measurements." J. Fluid Mech., 924(A21). https://doi.org/10.1017/jfm.2021.632

Section 3

Ocean Surface Vector Wind Algorithm Description

3.1. Physical Basis and Purpose

Estimation of Ocean Surface Vector Winds (OSVW) from IWRAP utilizes Bragg scattering, wherein microwave signals resonate with capillary-gravity waves generated by surface wind stress. The objective is the characterization of ocean surface roughness via the Normalized Radar Cross-Section (NRCS, σ^0). This parameter facilitates the retrieval of U_{10N} (equivalent neutral wind speed at 10 m altitude), which is essential for characterizing air-sea momentum flux and surface stress governing tropical cyclone thermodynamics.

The IWRAP OSVW product complements the 3D wind retrieval by providing an independent estimate of surface wind speed and direction derived directly from the ocean surface backscatter, rather than from precipitation volume Doppler measurements. This dual-retrieval capability provides internal consistency checks and extends the measurement portfolio of the NOAA WP-3D platform.

3.2. Geophysical Model Function (GMF) Inversion

The algorithm inverts observed NRCS using an empirical Geophysical Model Function (GMF):

$$\sigma^0 = A_0(U_{10n}, \theta)[1 + a_1(U_{10n}, \theta)\cos\chi + a_2(U_{10n}, \theta)\cos 2\chi]$$

where σ^0 is the normalized radar cross-section, U_{10N} is the equivalent neutral wind speed at 10 m altitude, θ is the incidence angle, χ is the wind-relative azimuth angle, A_0 is the mean NRCS, and a_1 and a_2 are the Fourier coefficients representing the upwind/downwind and upwind/crosswind backscatter modulation, respectively. The GMF coefficients are derived empirically from collocated IWRAP NRCS observations and independent wind measurements (dropsondes, SFMR, buoys).

Research using the IWRAP radar system identified co-polarized (VV/HH) NRCS saturation at hurricane-force winds exceeding approximately 35 m/s (Fernandez et al., 2006). This saturation is attributed to the transition from a capillary-wave dominated surface to a foam- and spray-dominated regime at extreme winds, where the relationship between wind speed and surface roughness fundamentally changes. Cross-polarized (VH) NRCS measurements, however, continue to increase monotonically with wind speed up to at least 70 m/s, providing a non-saturating signal for extreme wind estimation (Sapp, 2015; Sapp et al., 2016).

3.3. Unified 10 m Ocean Surface Wind Vector Product

A unified 10 m OSVW product is generated by combining scatterometry-derived OSVW with the lowest-level 3D Doppler wind estimates, adjusted to 10 m height. This blended approach exploits the complementary strengths of both retrieval methodologies:

- **In rain rates exceeding 10 mm/hr:** The 3D Doppler wind at the lowest available altitude is used, as scatterometry retrievals are degraded by atmospheric attenuation and surface splash effects.
- **In rain rates below 3 mm/hr:** Scatterometry OSVW is used, as it provides a direct measurement of the ocean surface roughness response to wind stress without dependence on precipitation backscatter.
- **In intermediate rain rates (3–10 mm/hr):** Scatterometry winds are flagged for reduced confidence, and a gap exists that requires further investigation. Filling this gap necessitates correcting the surface backscatter for rain attenuation and volume scattering effects.

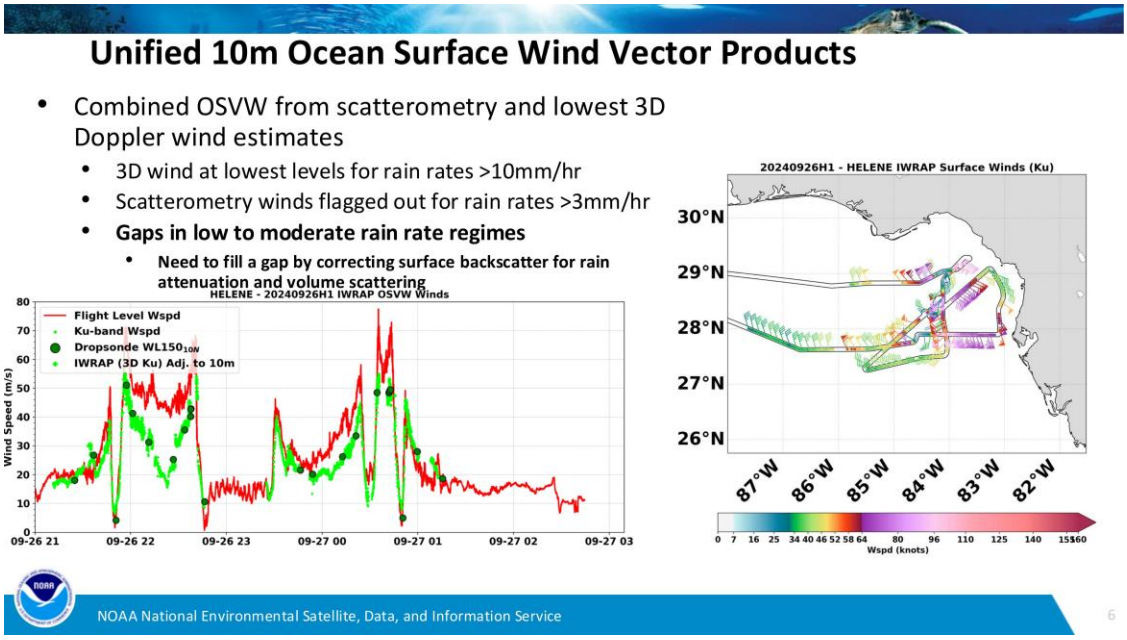

Figure 3.1: Unified 10 m OSVW product for Hurricane Helene (2024). Left: time series of flight-level wind speed (red), Ku-band scatterometry OSVW (green), dropsonde winds (green circles), and IWRAP 3D lowest-level winds adjusted to 10 m (blue). Right: spatial map of IWRAP Ku-band surface winds along the flight track. The blended product combines scatterometry in clear-air regimes with 3D Doppler winds in precipitating regions.

3.4. Precipitation Effects on Scatterometry

Precipitation complicates OSVW retrievals through two principal mechanisms: atmospheric attenuation of the radar signal along the propagation path, and the "splash effect" (impact-induced surface roughening) at the ocean surface. Two-way loss is corrected using path-integrated attenuation derived from the precipitation reflectivity profile measured by IWRAP.

The spectral processing methodology provides a unique opportunity to quantify and correct rain effects on scatterometry. In conventional pulse-pair processing, the measured NRCS (σ^0) includes contributions from the surface, atmospheric attenuation, and volume scattering from rain. In spectral processing, the rain volume backscatter can be separated from the surface signal in

Doppler space, yielding a cleaner surface NRCS estimate. The difference between pulse-pair and spectrum-derived σ^0 quantifies the rain contamination, enabling development of improved rain correction algorithms for satellite scatterometers such as ASCAT, OSCAT, and SAR.

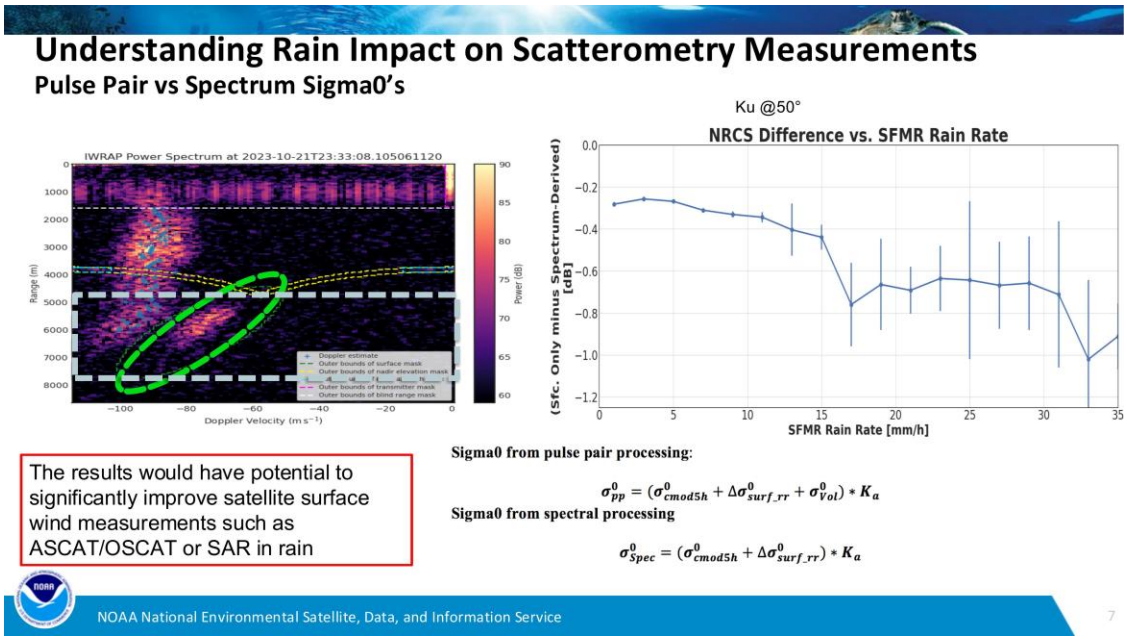

Figure 3.2: Understanding rain impact on scatterometry measurements. Left: IWRAP Ku-band power spectrum showing the separation between surface and rain volume signals. Right: NRCS difference between pulse-pair and spectrum-derived σ^0 at Ku-band 50° as a function of SFMR rain rate, demonstrating increasing contamination with rain rate. These results have the potential to significantly improve satellite surface wind measurements from ASCAT/OSCAT or SAR in rain.

Investigations by Carswell et al. (2010) and Contreras et al. (2007) indicate that for C-band at incidence angles between 22° and 50°, the splash effect is secondary to the wind-driven capillary wave response. At Ku-band, the rain-induced effects are more significant due to both increased atmospheric attenuation and enhanced surface perturbation. The dual-frequency design of IWRAP enables quantification and separation of these precipitation effects by comparing the C-band and Ku-band surface returns under identical environmental conditions (Fernandez et al. 2005).

3.5. Satellite Risk Reduction and MetOp-SG Synergy

The IWRAP OSVW research program serves as a critical validation and risk-reduction platform for the next-generation European Meteorological Operational Satellite—Second Generation (MetOp-SG) scatterometer (SCA). IWRAP's multi-frequency, multi-polarization, multi-incidence-angle measurement capabilities closely replicate the observation geometry planned for SCA, making it an ideal surrogate for pre-launch algorithm development.

Research has characterized the cross-polarized (VH) NRCS response to extreme winds, demonstrating that the VH signal maintains sensitivity to wind speed up to at least 70 m/s without

exhibiting the saturation observed in co-polarized channels (Sapp et al. 2016, 2018). IWRAP was utilized to test prototype antenna hardware and signal processing algorithms for MetOp-SG, directly informing design requirements for future satellite sensors to resolve hurricane-force winds. The IWRAP measurements provide the only extensive dataset of dual-polarization ocean surface backscatter at C-band and Ku-band in tropical cyclone conditions, constituting an essential reference for satellite scatterometer calibration and validation.

3.6. References

Carswell, J., E. Knapp, M. Goodberlet, and P. Chang. 1999. "Active/Passive Remote Sensing of Ocean Wind Vector for Hurricane Reconnaissance Applications." Proc. IEEE IGARSS, 3: 1854–1856. https://doi.org/10.1109/IGARSS.1999.772117

Carswell, J. R., Perkovic, D., Chu, T., Frasier, S. J., Chang, P., and Jelenak, Z. 2010. "Preliminary Investigation of Splash Effect on High Wind C-band HH-pol Model Function." Proc. 2010 IEEE Int. Geosci. and Remote Sens. Symp. IGARSS 2010. https://doi.org/10.1109/IGARSS.2010.5651890

Contreras, R. F., Frasier, S. J., Esteban-Fernandez, D., and Chang, P. 2007. The effect of rain on retrieval of C- and Ku-band scatterometer surface winds during Hurricanes Lili (2002) and Isabel (2003). Geoscience and Remote Sensing Symposium (IGARSS), 2007 IEEE International, 4463–4466. https://doi.org/10.1109/IGARSS.2007.4423846

Dvorsky, J. 2012. "Implementation of Dual-Polarization on an Airborne Scatterometer." MS Thesis, University of Massachusetts Amherst. http://scholarworks.umass.edu/theses/743

Fernandez, D. E., P. S. Chang, J. R. Carswell, R. F. Contreras, and S. J. Frasier, 2005. "Airborne measurements of rain and the ocean surface backscatter response at C- and Ku-band." Geoscience and Remote Sensing Symposium (IGARSS), 2005 IEEE International. https://doi.org/10.1109/IGARSS.2005.1526162.

Fernandez, D. E., J. R. Carswell, S. Frasier, P. S. Chang, P. G. Black, and F. D. Marks, 2006. "Dual-polarized C- and Ku-band ocean backscatter response to hurricane-force winds." J. Geophys. Res., 111(C8), https://doi.org/10.1029/2005JC003048.

McLaughlin, D. J., R. E. McIntosh, A. Pazmany, L. Hevizi, and E. Boltniew. 1991. "A C-band Scatterometer for Remote Sensing the Air-Sea Interface." IEEE Trans. Geosci. Remote Sens., 29(2): 260–267. https://doi.org/10.1109/36.73667

Sapp, J. W., S. J. Frasier, J. Dvorsky, P. S. Chang, and Z. Jelenak, 2013: Airborne Dual-Polarization Observations of the Sea Surface NRCS at C-Band in High Winds. IEEE Geosci. Remote Sens. Lett., 10(4), 726–730, https://doi.org/10.1109/LGRS.2012.2220118.

Sapp, J. W. 2015. "Improving Sea-Surface Remote Sensing of Ocean Wind Vectors by Scatterometers." PhD Dissertation, University of Massachusetts Amherst. https://doi.org/10.7275/7433226.0

Sapp, J., P. Chang, Z. Jelenak, S. Frasier, and T. Hartley, 2015. "Sea-surface NRCS observations in high winds at low incidence angles." Geoscience and Remote Sensing Symposium (IGARSS), 2015 IEEE International, Milan, Italy, 1199–1202, https://doi.org/10.1109/IGARSS.2015.7325987.

Sapp, J. W., S. O. Alsweiss, Z. Jelenak, P. S. Chang, S. J. Frasier, and J. Carswell, 2016. “Airborne Co-polarization and Cross-Polarization Observations of the Ocean-Surface NRCS at C-Band.” IEEE Trans. Geosci. Remote Sens., 54(10), 5975–5992, https://doi.org/10.1109/TGRS.2016.2578048.

Sapp, J., P. Chang, Z. Jelenak, S. Frasier, and T. Hartley, 2016. “Cross-polarized C-band sea-surface NRCS observations in extreme winds.” Geoscience and Remote Sensing Symposium (IGARSS), 2016 IEEE International, Beijing, China, 2243–2246, https://doi.org/10.1109/IGARSS.2016.7729579.

Sapp, J., Z. Jelenak, P. Chang, and S. Frasier, 2018. “C-Band Cross-Polarization Ocean Surface Observations in Hurricane Matthew.” 2018 IEEE International Geoscience and Remote Sensing Symposium (IGARSS), 2018 IEEE International Geoscience and Remote Sensing Symposium (IGARSS), 5595–5598, https://doi.org/10.1109/IGARSS.2018.8519433.

Sapp, J. W., A. A. Mouche, Z. Jelenak, P. S. Chang, and S. J. Frasier, 2020. “Comparison of the Sentinel-1B Synthetic Aperture Radar With Airborne Microwave Sensors in an Extra-Tropical Cyclone.” IEEE Trans. Geosci. Remote Sens., 58(7), 4721–4729, https://doi.org/10.1109/TGRS.2020.2966332.

Sapp, J. W., Z. Jelenak, P. S. Chang, and J. R. Carswell, 2023. “Frequency Agility Implementation in the Imaging Wind and Rain Airborne Profiler (IWRAP) Instrument.” IGARSS 2023 - 2023 IEEE International Geoscience and Remote Sensing Symposium, IGARSS 2023 - 2023 IEEE International Geoscience and Remote Sensing Symposium, Pasadena, CA, USA, IEEE, 4352–4355, https://doi.org/10.1109/IGARSS52108.2023.10283169.

Sapp, J. W., Z. Jelenak, P. S. Chang, S. R. Guimond, and J. R. Carswell, 2025. “Near-Real-Time IWRAP 3D Wind Retrievals.” Trans. Rad. Sys., 3, 832--842, https://doi.org/10.1109/TRS.2025.3563787.